Real-time measurements of crystallization processes in viscoelastic polymeric photonic crystals

David R. E. Snoswell,[1,*] Chris E. Finlayson,[2,†] Qibin Zhao,[1] and Jeremy J. Baumberg[1,‡]
[1]*Cavendish Laboratory, University of Cambridge, Cambridge CB3 0HE, United Kingdom*
[2]*Department of Physics, Prifysgol Aberystwyth University, Aberystwyth, Wales SY23 3BZ, United Kingdom*
(Received 12 September 2014; revised manuscript received 17 April 2015; published 30 November 2015)

We present a study of the dynamic shear ordering of viscoelastic photonic crystals, based on core-shell polymeric composite particles. Using an adapted shear-cell arrangement, the crystalline ordering of the material under conditions of oscillatory shear is interrogated in real time, through both video imaging and from the optical transmission spectra of the cell. In order to gain a deeper understanding of the macroscopic influences of shear on the crystallization process in this *solvent-free* system, the development of bulk ordering is studied as a function of the key parameters including duty cycle and shear-strain magnitude. In particular, optimal ordering is observed from a prerandomized sample at shear strains of around 160%, for 1-Hz oscillations. This ordering reaches completion over time scales of order 10 s. These observations suggest significant local strains are needed to drive nanoparticles through energy barriers, and that local creep is needed to break temporal symmetry in such high-viscosity nanoassemblies. Crystal shear-melting effects are also characterized under conditions of constant shear rate. These quantitative experiments aim to stimulate the development of theoretical models which can deal with the strong local particle interactions in this system.

DOI: 10.1103/PhysRevE.92.052315 PACS number(s): 83.50.−v, 61.41.+e, 78.66.Sq, 81.05.Lg

I. INTRODUCTION

Photonic structures based on colloidal crystals, in which periodic variations in refractive index create photonic band gaps, have attracted considerable attention in recent years. Colloidal crystals can be fabricated by self-assembly of submicron-sized monodisperse spheres, typically made of polystyrene or silica [1–4]. Because the spheres are of a diameter comparable to the wavelength of light, there is potential for the development of structured materials with distinguishing optical properties, which are not accessible using dyes or pigments, particularly if the colloidal particles become highly ordered. Layers of close-packed spheres generate a periodic refractive index variation with the wavelength of maximum reflection λ_{max} from the colloidal crystal dependent on the layer spacing, incident angle, and refractive index contrast according to the well-known Bragg law.

In recent work, we have reported three-dimensional (3D) ordered polymeric photonic crystals or "polymer opals" [5–9]. These are fabricated by shear-induced ordering of core-interface-shell (CIS) structured polymer spheres. The CIS polymer sphere is composed of a rigidly cross-linked polystyrene (PS) core (i.e., a rigid spherical core) covered with a low–glass transition temperature (T_g) poly(ethyl acrylate) (PEA) soft shell, via a thin (∼10 nm) poly(methyl methacrylate) (PMMA) interlayer containing the comonomer allyl methacrylate (ALMA) as a grafting agent [Fig. 1(a)]. Synthesis of CIS spheres is achieved by an emulsion polymerization route and the overall CIS diameter is readily controllable, typically ranging from 150 to 350 nm, without affecting the high monodispersity [5,10]. The Bragg wavelength can thus be readily tuned over the whole range of the visible and near infrared spectral region by adjusting the sphere size. The net relative refractive index contrast ($\Delta n/n$) between core and shell materials in the archetypal PS-PEA system is typically of order 7%. Rheological studies [11,12] have demonstrated that, while remaining grafted to the core, the soft shell polymer forms a quasicontinuous viscoelastic matrix during the shear-ordering process and the rigid spheres become regularly arranged. The final solvent-free polymer opals show exceptional flexibility, mechanical robustness, and stretchability (>100%), along with the possibility of tuning the optical properties by viscoelastic deformation [6,13]. These samples thus allow access to an exceptional variety of experiments (and the associated scientific insights) which are mechanically impossible in more conventional monolithic photonic crystals.

The development by Finlayson *et al.* of an edge-induced rotational shearing (EIRS) process [14] has been demonstrated to reproducibly produce samples with improved uniformity of 3D bulk ordering over areas of square meters and through film thicknesses of greater than 100 microns, greatly enhancing both the intensity and chromaticity of the observed structural color. Multiple crystallographic and microscopic characterizations [14,15] have confirmed a cubic packing structure, with the absence of next-nearest-neighbor interactions producing a random hexagonal packing arrangement. The subsequent demonstration of scale-up of these elastomeric synthetic opaline films to industrial length scales makes them very attractive as a route to a wide range of large-area and bulk-scale photonics applications, offering a step change away from the monolithic architectures which are currently relied upon, including photonics materials, coatings, fibers, and sensors [16–20].

While the efficacy of shear-induced ordering in polymer opals has been demonstrated, relatively little is known concerning the detailed mechanism or time dependence of photonic crystal formation. In other systems of shear assembly of micron-sized particles, such as the low-viscosity colloidal suspensions described by Ackerson *et al.* [21,22], Amos *et al.* [23], and Liu *et al.* [24], crystallization rates and the influence of conditions and experimental parameters have been

*DSnoswell@slb.com
†cef2@aber.ac.uk
‡jjb12@cam.ac.uk

 ©2015 American Physical Society

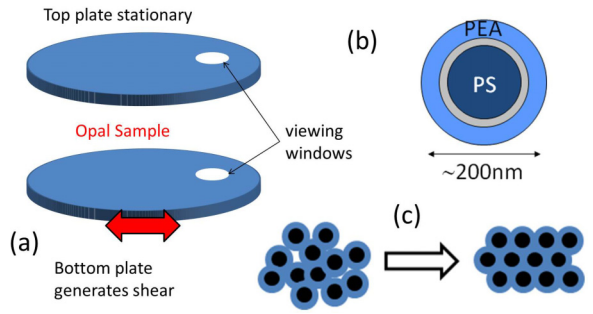

FIG. 1. (Color online) (a) Experimental geometry used in shear-cell measurements, with opal sample introduced between two plates with optical viewing windows. Shearing of the sample is achieved by the relative rotational motion of the plates; the strain in all subsequent experiments is defined at the point of observation in the (middle of the) viewing window, which is offset from the center. (b) Core-shell architecture of precursor particles, (c) self-assembled into polymer opals.

characterized to a significant degree. More recent studies have also described the effects of oscillatory shear in such systems [25,26], where continuous shear can crystalize colloids when there is a fluid medium present.

However, we emphasize that these systems of colloidal suspensions cannot be directly compared to polymer opals, which in fundamental contrast contain *no solvent*. The core-shell design of particles means that, even at the point of melting, the polymer opals do not contain a discrete fluid phase. Commensurately, the system is athermal, and mobility of the spheres is highly inhibited by the gumlike medium. There is strong dissipation inside the system due to the viscoelasticity of the PEA and no diffusive Brownian motion is shown to exist; therefore the system does not have the ability to self-assemble. The characteristic Peclet number, $P_e = \gamma a^2/D_0$ (where γ is the shear rate, a the particle radius, and D_0 the Stokes-Einstein diffusion coefficient) [27] in the opals is therefore consistently very much greater (of order a millionfold) than in the colloidal suspensions. While many of the studies into ordered colloids therefore produce metastable crystallization states, the structures reported here represent stable configurations, as confirmed experimentally [5–20]. The colloidal systems are also entropy driven and equilibrium structures are determined by a resultant potential energy minimum from a combination of interparticle collisions, dispersive forces, and electrostatic forces, etc. [28]. By contrast, the equilibrium in polymer opals is mainly associated with the accumulation and release mechanisms of strain energy from external forces, e.g., shearing, stretching, etc. In such a system, where the fluid is absent, particles can additionally exert torque on each other. No theoretical understanding of this ordering yet exists, despite its utility in creating very large-scale ordered nanostructures.

In this paper, we present real-time measurements of dynamic shear ordering and crystallization, thus gaining a deeper temporal understanding of the processes in polymer opal formation. An adapted oscillatory shear cell facilitates a study of the macroscopic influences of shear on the crystallization process, and the development of bulk ordering is studied as a function of key experimental parameters, such as duty cycle and strain magnitude.

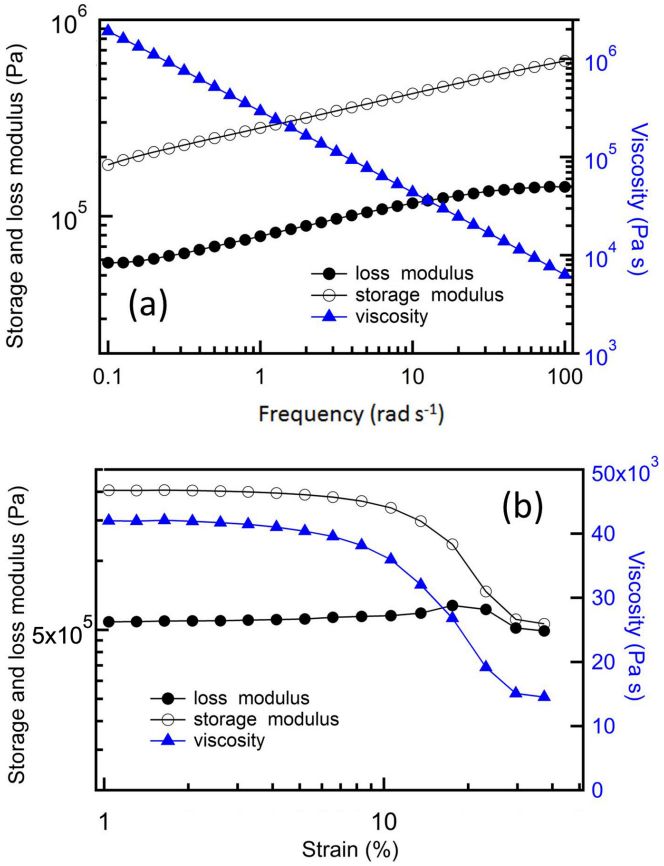

FIG. 2. (Color online) Storage and loss moduli, and the viscosity of polymer opal material, obtained using an ARES-G2 rheometer. Data are shown in (a) as a function of strain-shear oscillation frequency (temperature of 100 °C), and in (b) as a function of strain magnitude (temperature of 100 °C and an oscillation frequency of 10 rads/s). The polymer opal sample characterized here has a representative core-shell particle size of ≈250 nm, and $T_{glass} \approx -15$ °C.

II. METHODOLOGY AND SAMPLES

The polymer opal material described in this paper is based on ensembles of core-interlayer-shell (CIS) particles, as illustrated in Fig. 1. These were synthesized using a multi-stage emulsion polymerization process, as previously reported [5,29]. The core-shell particle precursors are approximately 250 nm in diameter, and consist of a hard cross-linked polystyrene (PS) core, coated with a thin polymer layer containing Poly(methyl methacrylate) as a grafting agent, and a soft polyethylacrylate (PEA) outer shell [10]. In this configuration, the net refractive index contrast between core and shell material is $\Delta n \approx 0.11$, and the volume fraction of cores ≈55%. A general overview of the standard measured rheological parameters of the resultant polymer opal material is given in Fig. 2. In particular, the general signatures of viscoelastic behavior are observed, with the convergence of the storage and loss plots at strains around 20%–30%, indicating the yield point, as is consistent with our earlier reports [13,18]. Low oscillation frequency viscosities are in the range of 10^5–10^6 Pa s, even at 100 °C.

TABLE I. The standard four-step shear sequence used in the characterization of opal samples. The mode of shearing, interplate gap, strain, shear rate (calculated from the local shear velocity, which equals lateral speed divided by thickness), oscillation frequency, and cycle time are shown for each of the four steps.

Step	Mode of shear	Gap (μm)	Strain	Shear rate (s^{-1})	Frequency (Hz)	Time (s)
1 (Randomize)	continuous	300	n/a	2	n/a	10
2 (Stress relaxation)	continuous	300	n/a	0.1	n/a	10
3 (Crystal growth)	oscillatory	300	200%	2	1	10
4 (Stress relaxation)	oscillatory	300	50%	4	2	10

The shear cell (Linkham CSS450 model [30]) used in these optical interrogation experiments is illustrated in Fig. 1. The CIS precursor batch in this case was engineered for rheological testing at a slightly reduced Peclet number compared to that for the opals previously studied; the shell PEA material was 2.5% thiolated, giving both a measured T_{glass} value some 10 °C lower. In the present samples, no additional pigments (such as carbon black nanoparticles) were added, to avoid additional spectral complexity, such as the peculiar angular dependence noted in some earlier studies [31,32]. The as-synthesized composite material is carefully encapsulated between two parallel circular quartz windows with radius 1.5 cm and spacing 300 μm, giving a total sample volume of $\sim$0.2 μl. Viewing ports of radius 1.4 mm are built into each supporting plate at a radius of $\sim$1 cm from the center of the quartz windows. The viewing ports are in an overlapping arrangement such as to allow continuous optical transmission measurements of the sample. Shearing of the sample is then achieved by a mechanical rotation of the bottom quartz window; the top quartz window is fixed stationary. As the cell is of a circular geometry, this arrangement thus provides only an approximation of linear shear. However, the strain in all subsequent experiments is thus defined at the point of observation in the (middle of the) observation window, which is offset from the center [30]. To achieve the necessary viscoelastic response, the cell is heated to a fixed temperature of 100 °C.

Samples were tested in the shear cell using the standard cycle given in Table I. Firstly, a single continuous shear at constant rate over 10 s is employed to "randomize" the sample and establish a base condition from which ordering can be initiated. In practice continuous shear is achieved by rotating the bottom plate in a clockwise direction. Secondly, a much slower shear rate in the same direction over 10 s relaxes any residual elastic forces present. Thirdly, oscillatory shearing (frequency 1 Hz, shear-strain amplitude 200%, or $\delta l/d \approx 2$, where δl is the displacement of the cell plates and d is the sample thickness) is used to "crystallize" the opal via shear ordering. Ideally removing the shear stress required for crystallization will have no detrimental effects on ordering, but this may depend upon the phase when the oscillatory shear is stopped and the amount of stored elastic energy at the instant oscillation ceases. To relieve these elastic stresses, final small-amplitude oscillation (frequency 2 Hz, strain amplitude 50%) is employed to negate any residual phase dependence in the previous shear-ordering phase. One might anticipate the same problem of phase also occurs during this step, but on a much reduced scale.

Real-time spectroscopic measurements were taken with an adapted Olympus BX51 microscope, using an incandescent white light source focused to a spot size of approximately 10 μm diameter (5× magnification), with the optical signal collected using suitable focusing optics and a fiber-coupled CCD spectrometer. The spectra were normalized using a diffusive white-light scatterer (for dark-field reflectance) and by using appropriate control measurements of the empty cell (for transmittance). All the microscopic images displayed were then taken with an Olympus BX51 light microscope, with videos being recorded on an RGB format video camera with pixel resolution set to 800 × 600 and a video white balance of red 2.41, green 2.03, blue 3.89, gain 1.1. Data was taken in transmission mode, instead of reflectance, for two main reasons. Firstly, the transmission yields information about light which has propagated across the bulk 300-μm thickness of the sample, whereas the reflectivity is only representative of ordering down to depths $\sim$10 μm. Secondly, as we are not measuring freestanding films as in Ref. [14], but material embedded between optical windows, there are practical issues of specular reflections from the windows and the normalization of spectra to overcome in reflectance.

III. RESULTS

In Fig. 3(a), optical transmission spectra are shown as taken from the first phase of the testing cycle showing the randomization of a crystalline phase through continuous shear. Initially, the spectrum shows a marked *stop-band* resonance centered around $\lambda = 600$ nm, with higher transmittance at both the low- and high-energy sides. The reduced transmission at the UV end of the spectra is simply due to increased absorption at short wavelengths in the glass optics used. As the preshear phase develops spectra are captured at 0.2-s intervals, illustrating the shear melting of the crystal from an ordered to a disordered state over a time scale of 3 s. This may be inferred from the rapidly decreasing Q factor of the resonance and the commensurate change in transmission at the low-wavelength side of the resonance, which is directly indicative of the change in the particle spacing (radial distribution function) in the crystal [33]. Hence, characterizing this short-wavelength end (around $\lambda = 530$ nm) enables us to directly correlate spectral changes to increased or decreased ordering. To thus analyze how this shear melting of the opaline crystal progresses, in Fig. 3(b) the transmittance at $\lambda = 530$ nm is extracted as a function of shearing time. Qualitatively, it was observed that the data showed an asymptotic behavior both at short and long times, and it is found that a sigmoidal function provides a good

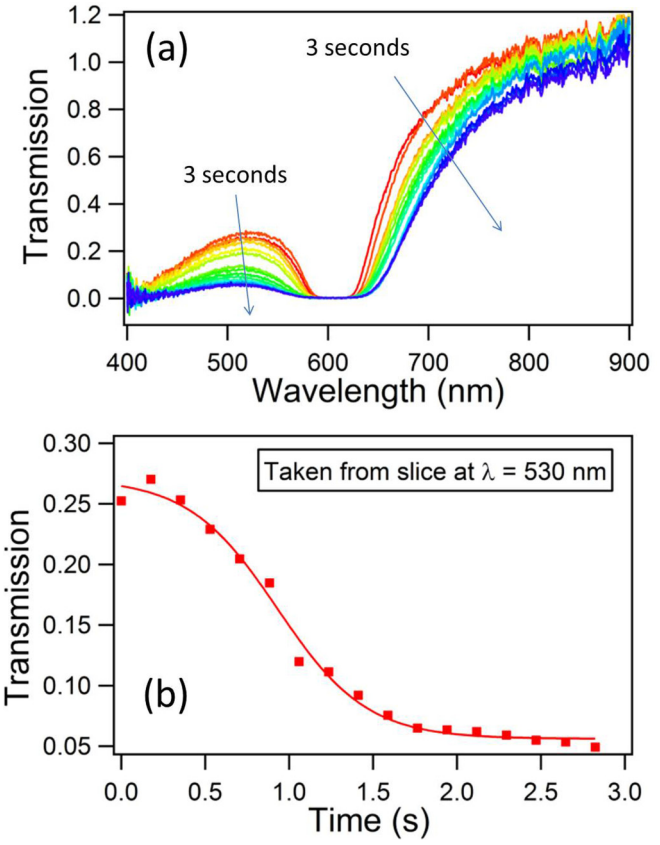

FIG. 3. (Color online) (a) Optical spectra taken from the preshear phase of an opal sample, showing the shear melting of the crystal over 3 s. (b) Transmittance at $\lambda = 530$ nm as a function of shearing time. The points are fitted to a sigmoid function to extract a decay time.

empirical fit. It is seen that the shear melting is at near total completion in these experiments.

Conversely, in Fig. 4(a) optical spectra taken during the crystallization (oscillatory shear at 1 Hz) phase of the testing cycle are shown. The progress of crystallization at 0.1-s intervals over a period of 10 s is observed, as inferred from the change in transmission at the low-wavelength side of the resonance. Further qualitative analysis of the crystallization process may be gained from the corresponding semilog plot [Fig. 4(b)], showing the development of the photonic stop band with increasing Q factor of resonance. The small, yet measureable, progressive redshifting of the resonance with increasing ordering is also consistent with previous reports [14], whereby the in-plane packing density increases, thus pushing the crystal layers apart.

In order to gain a better insight into the dynamics of crystal formation, the data are now plotted as extinction coefficient (at $\lambda = 530$ nm) against time. The effective extinction coefficient (α) is here empirically defined as

$$\alpha = \frac{-\ln(T)}{d}, \tag{1}$$

where T is transmittance and d is the sample thickness [see Fig. 4(c)]. In this form, the data can readily be fitted to an exponential function of the form

$$\alpha(t) = \alpha_0 + Ae^{-t/\tau}, \tag{2}$$

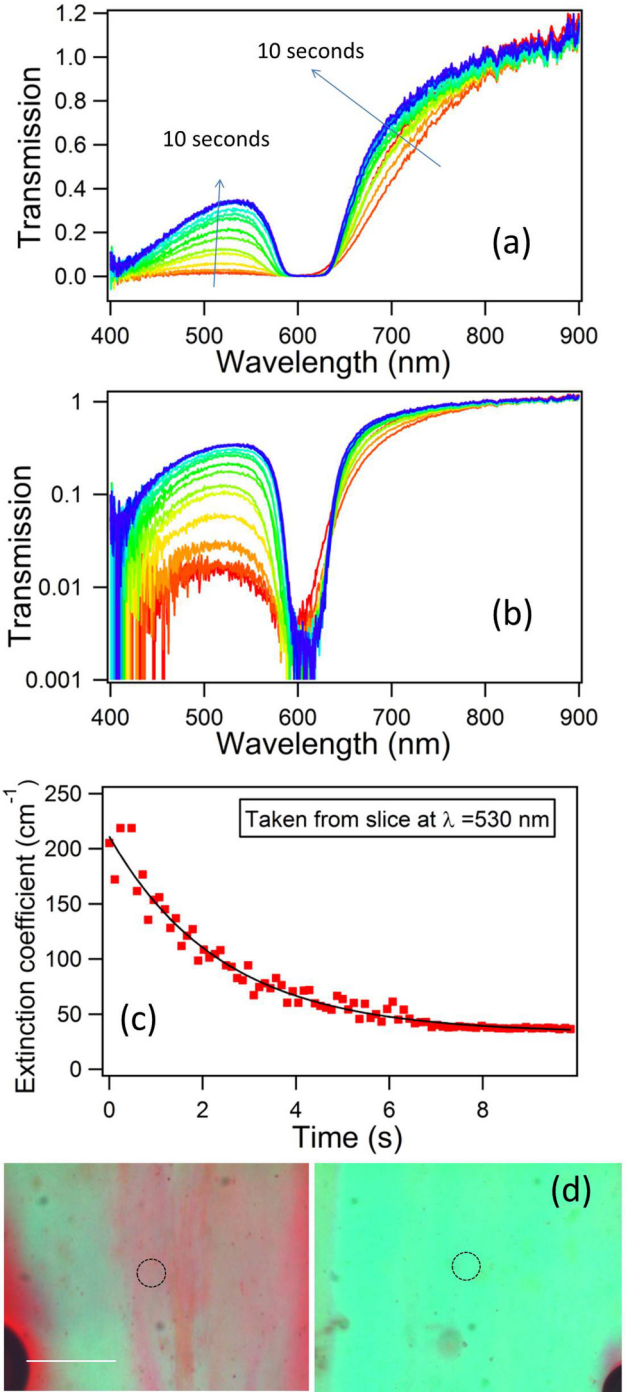

FIG. 4. (Color online) (a) Optical spectra taken during the crystallization of an opal sample by means of an oscillatory shear, showing the progress of crystallization over 10 s. (b) Corresponding semilog plot reveals detail of the spectral features present. (c) Optical extinction coefficient at $\lambda = 530$ nm as a function of shearing time, together with a fit to an offset exponential function, of lifetime $\tau = 2.4$ s. (d) Representative transmission microscope images; on the left is a sample (preoscillatory shear) where significant regions of poor crystalline ordering are evident at the moment of image capture. On the right, a sample with uniform ordering and an intense green structural color, following oscillatory shear, is imaged. In both cases, the magnification was 5× and the scale bar is ≈0.2 mm. The dashed circles on the images indicate the spot size over which spectra are obtained.

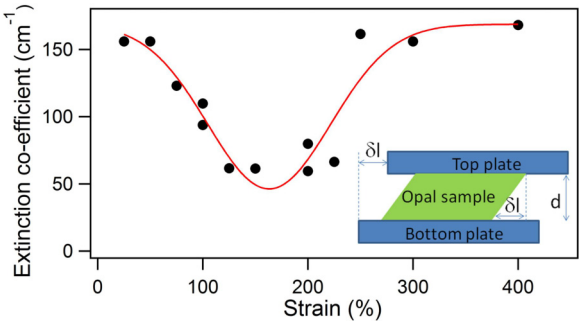

FIG. 5. (Color online) Crystallization of an opal sample, as inferred from the optical extinction coefficient at the low wavelength side of the resonance ($\lambda = 530$ nm), as a function of strain, given a shear cycle of oscillation frequency 1 Hz for 10 s. The data points are fitted to a Gaussian function to guide the eye, with the minimum value of optical extinction indicating that optimal crystalline ordering occurs at strain magnitudes of 160%. The inset defines the shear strain ($\delta l/d$) within the cell geometry as indicated.

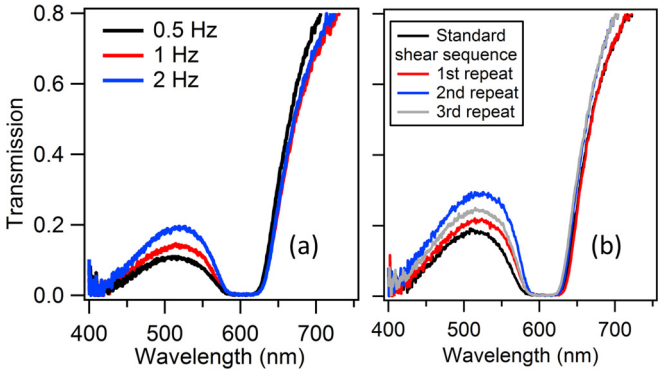

FIG. 6. (Color online) (a) Effect of variation of shear oscillation frequency on the end transmission spectrum, retaining other parameters from Table I, and using a strain magnitude of 75%. (b) Spectra after multiple repetitions of the standard four-step shear sequence.

where a_0 and A are offset constants and τ the time scale. Under these conditions of crystallization, a lifetime for the disorder-order transition of $\tau = 2.4$ s is extracted. The progress of crystallization may also be followed visually from the intense structural colors which result; representative transmission microscope images are given in Fig. 4(d) comparing a sample where significant regions of poor crystalline ordering are evident at the moment of image capture, with a sample with uniform ordering and an intense green structural color, following oscillatory shear. Two videos, which illustrate these visible changes in real time, are also available in the Supplemental Material [34]. We note that some imperfections are evident in the images and videos taken over wide sample regions, associated with localized contaminants, cavities, and edge effects. However, care is exercised in ensuring uniformity over the areas from which spectra are gathered. The structural color (and spectra) arising from disordered regions are self-evidently very different from ordered regions, and thus easy to avoid. These videos also give a better context of the experimental dimensions, where the observation radius is 7.5 mm to the center of the viewing window (radius 1.4 mm). We expect that the strain therefore varies by $1.4/7.5 \times 100 = 18.7\%$ from one edge of the window to the other. Visually, there might indeed be signs of differences in crystallization between the edges, although this is masked to some degree by sample inhomogeneity. However, spectra are taken from a tiny spot (~10-micron diameter) in the middle of this frame, across which the strain only varies by 0.13%, which is insignificant in the wider context of the measurements.

As a further investigation into the dependence of the shear-ordering process on the magnitude of shear strain, samples were subjected to shear cycles (oscillation frequency 1 Hz, 10 s) for various linear strain values of up to 400%. As before, the degree of crystallization is inferred from the extinction coefficient at the low-wavelength side of the resonance ($\lambda = 530$ nm). As shown in Fig. 5, at low strain values below 100%, there is relatively little decrease of the low-λ optical extinction, indicating a limited, suboptimal development of crystallization. Strains in the range of ~100%–250%, however, produce much greater changes in the extinction coefficient, implying crystallization processes which are equilibrated or near complete. As the strain magnitude increases towards 400%, a significant rise then occurs in the low-λ extinction, indicating an above-optimal strain and a limited development of crystallization. While there is no obvious functional trend, in Fig. 5 the data points are fitted to a Gaussian-type function for clarity, indicating that optimal crystalline ordering occurs at a strain magnitude of around 160%. The residual extinction of $\approx 50\,\mathrm{cm}^{-1}$ at this wavelength must come from additional sources of scattering that cannot be removed through the shearing. Current experiments are unable to distinguish between inherent point and line defects induced by the shear process, or residual background scatter coming from sources other than the multiple periodic sphere interfaces. For instance these may include refractive index variations of the PEA polymer matrix, sphere size, or refractive index inhomogeneity, or other causes.

A study of the effect of oscillation frequency (within the experimentally attainable range of 0.5–2 Hz) gave no conclusive analysis (see Fig. 6), implying that using a higher frequency within a practicable range does not assist the crystallization. While there is apparently some slight improvement in the final ordering in going from 0.5 Hz up to 2 Hz, this might also be attributable to the increased number of cycles executed at higher frequencies. Within the 10-s "crystal growth" phase, as detailed in Table I, the number of successive cycles scales from 5 (at 0.5 Hz) up to 20 (at 2 Hz). A comparison may be drawn with Fig. 4, where at 1 Hz the characteristic time scale of 2.4 s corresponds to 2.4 shear cycles, and where an optimized structure is reached within 6–7 s (or 6–7 shear cycles).

Also, a key advantage of polymer opals as reported has been the ability to generate *permanent* structures in the solid state. While a comparable stability may also be observed in highly concentrated suspensions (above volume fraction of 50%) [25] and glasses of hard spheres [35], these cases produce structures without any of the other favorable attributes of polymer opals, such as viscoelasticity, mechanochromism, and bulk scalability. Normally colloidal crystals formed by shear in a concentrated suspension would eventually dissolve by diffusion (depending on solid concentration and particle size). In spite of the lower viscosity of these samples as compared to

the thin films reported previously and the higher temperature of the melt, we still technically have a solventless "fluid" with high yield stress, and thermal rearrangement due to diffusion is negligible. The relaxation of elastic strain in the shell material is accelerated at higher temperatures and this may cause a slight disordering in the crystal; however, there is no evidence of such degradation with time due to thermodynamics (thermal motion). Once any elastic forces have been allowed to relax (phases 2 and 4 of the testing cycle; see Table I), the optical spectra of the resultant structures are not seen to change or degrade significantly over time scales of hours, while our previously reported polymer opal films notably retain their iridescence over time scales of several years [5–19]. This illustrates another key difference with shear-ordering colloidal systems within a fluid phase [21–28], where a minimum shear rate is required for crystallization to remain, and thermal motion rapidly produces dissolution at rest.

The reproducibility of shear ordering after several standard shear cycles was also tested (see transmission spectra in Fig. 6). Each repeat cycle produced crystalline ordering, as characterized from the transmission spectrum, which was comparable to those above.

IV. DISCUSSION

The clear progression of crystallization in time with oscillatory shearing is wholly consistent with our earlier reports, which involved tracking the increased ordering using incremental multipass methods [11,14]. These earlier methods involved PET-encapsulated samples, with shear being applied by means of a heated edge or knife. In terms of the reproducible and uniform application of shear strain, the repeatability of the shearing cycle, and the lack of ability to perform *in situ* measurements in real time, these reports therefore had clear limitations. A linear dependency of ordering with number of shear passes (number of passes $\leqslant 5$) was proposed in Ref. [14]; however, physical intuition suggests that the optical signatures of ordering will not proceed indefinitely, but will reach an asymptotic limit at a time where crystallization has completed. Furthermore, it is to be expected that as the crystal becomes more "perfect," it will become more susceptible to damage by further motion. There should therefore be an equilibrium point at which the rate of damage (increasing defects) is equal to the rate of crystallization. This expected behavior is now strongly verified, as illustrated in Fig. 4.

We can make key quantitative comparisons with the many reports, both experimental and theoretical, of crystallization in colloidal suspensions [36,37]. A measured viscosity of $\sim 10^5$ Pa s within the oscillation frequency range of 1–10 Hz (Fig. 2) implies a diffusion coefficient at 100 °C of $D_0 \sim 1 \times 10^{-16}\,\mathrm{cm^2\,s^{-1}}$, according to the Einstein-Stokes relation for diffusion of spherical particles [38]. Taking into account the shear rates of order $1\,\mathrm{s^{-1}}$, and the particle radius of $\approx$125 nm, this value of D_0 implies a Peclet number of at least 10^6. In Panine *et al.*, crystallization in a suspension of latex particles is characterized under varied conditions of shear stress and oscillation frequency, although not as a function of amplitude [39]. In a comparable regime of stress vs. strain and frequency (1–10 Hz) to those reported in the manuscript, crystallization was observed to proceed on time scales of tens of seconds to minutes. The relaxation behavior of the structure on the cessation of shear was markedly different. Of particular note is that the Peclet numbers quoted in that work were in the range of 0–60, some five to six orders of magnitude lower than in the present report.

Of further interest is the dynamics of crystal shear melting under a constant shear rate (Fig. 3) and the apparent non-linearity at the beginning of the shear-ordering phase. It is clear that this also has a net effect on the overall time scale associated with the order-disorder transition in the crystal. One can speculate that there is an inherent yield stress in the system; the opals have to be sheared past a certain strain to produce viscoelastic flow. Previous microscopy studies on polymer opal films have revealed a layered cross section with ordered regions towards the outer surfaces [7,12], behavior which was also readily observed in the radial profile of extruded polymer opal fibers [40]. In the present situation, where shearing induces *disordering*, it could be that initially all the shear occurs at the cell walls, and then gradually propagates towards the middle of the cell. Alternatively, this could be evidence of an intrinsic non-Newtonian behavior, such as shear working or softening. Detailed rheological studies will be required in the future in order to fully address such issues.

In order to better analyze the dependency on strain magnitude (Fig. 5), it is instructive to refer to our previous work (Kontogeorgos *et al.* [13]) where the optomechanical properties of an ordered polymer opal film were investigated under the effect of a linear strain. While care must be taken in making a direct quantitative comparison of shear strain in these two distinct geometries, in that earlier case a correlation was found between the yield strain ($\sim$20%) and the slippage of crystal planes and the development of a phase change in the lattice structure. Hence, it can be inferred that straining the opal beyond the point of plane slippage enables a reconfiguration of particles into a more highly ordered configuration. As a further confirmation of the role of shearing in the ordering process, the work in Ref. [14] found that such shear-induced ordering required a minimum local strain, as defined by the curvature of the heated shearing edge. Once again, in the present study of oscillatory shear, we observe a strong dependency on the strain magnitude, with a marked "switch-on" of the crystalline ordering above $\sim$100% strain. Strains exceeding 100% seem thus to be required to drive the particles through local energy barriers.

During shearing of the polymer opal, momentum is transferred between spheres by collision and also by the elastic forces between matrix and spheres. As a general principle, when any work is done against these elastic forces (such as by shear), there must be a stored energy, which may be released either by (i) relaxation into the original state, (ii) relaxation into a more ordered state, or (iii) dissipated into the matrix due to the viscosity component of its stress response. It is expected that the transition from disorder to order will involve a change in the configurational energy, with an activation energy which is determined by the forces retaining the structure in its original state (the "restoring" force). For crystallization to proceed, the stored energy must be greater than this required activation energy [41]. Hence, a large shearing force gives more energy to sphere rearrangement, while the activation energy threshold is constant; therefore, we can infer that a

large strain is able to both increase the speed of crystallization and the equilibrium level of ordering. In this highly viscous system, temporal asymmetry seems to require that strain rates are comparable to local creep rates, thus suggesting an upper limit to the ordering speed possible.

This shear-cell study also facilitates investigation of the ordering behavior at much larger strain magnitudes than previously practicable. The crystalline ordering decreases rapidly above ∼250% shear strain. A comparable effect has also been seen in our previous work on stretching in polymer opal fibers [40]. We believe this to be an example of high-shear disorder (see Catherall *et al.* [42]), whereby the shear-induced movement and flow of particles at very high strain leads to a rapid breakdown of any crystalline ordering, and this also inhibits the crystallization of the opal from the base-disordered condition. Finally, in addition to crystallization processes in polymer opals, crystal shear-melting effects have also been characterized. The mechanism is suggested to be the introduction of disorder by the high strains produced from steady shear, as is consistent with our arguments concerning the shear-strain amplitude on ordering. In the present situation, where there is no fluid medium, it is to be expected that particle-particle friction is very high and can additionally transmit torque through the system, which is likely to be the main mechanism by which excessive shear causes shear melting.

V. CONCLUSIONS

By using an adapted shear-cell arrangement, we have presented a study of the dynamic oscillatory shear ordering of viscoelastic photonic crystals (polymer opals). The behavior of this solvent-free system is inherently distinct from that seen in shear-ordered colloidal suspensions within a fluid medium. The crystallization process, as inferred in real time from the optical transmission of the cell, shows an exponential-type behavior in the employed regime of viscosity, temperature, and shearing duty cycle, with time scales of order 2 s. The temporal dependence seen for crystal shear melting under large shear shows a marked nonlinearity in the early stage of the process, with a net effect on the overall associated time scale. An optimal ordering process is observed in a prerandomized sample at shear strains of around 160%, for a 1-Hz oscillation frequency. Clear regimes of suboptimal strain and high-shear disordering are observed at lower and higher amplitudes, respectively. One aim of this quantitative work is to stimulate and direct the development of theoretical models which can deal with the strong local particle interactions developed in this system, and which are needed to better harness the greatly improved nanoscale ordering they provide.

ACKNOWLEDGMENTS

The authors thank Professor Malcolm Mackley of the University of Cambridge for access to experimental equipment, and Professor Goetz Hellmann and Dr. Peter Spahn of Deutsches Kunststoff Institut (DKI) for provision of samples. This work is supported by EPSRC Grants No. EP/G060649/1, No. EP/E040241, and No. EP/H027130/1, and ERC Grant No. LINASS 320503.

[1] Y. A. Vlasov, X. Z. Bo, J. C. Sturm, and D. J. Norris, On-chip natural assembly of silicon photonic bandgap crystals, Nature **414**, 289 (2001).

[2] V. N. Astratov, A. M. Adawi, S. Fricker, M. S. Skolnick, D. M. Whittaker, and P. N. Pusey, Interplay of order and disorder in the optical properties of opal photonic crystals, Phys. Rev. B **66**, 165215 (2002).

[3] A. F. Koenderink, A. Lagendijk, and W. L. Vos, Optical extinction due to intrinsic structural variations of photonic crystals, Phys. Rev. B **72**, 153102 (2005).

[4] S. A. Asher, J. M. Weissman, A. Tikhonov, R. D. Coalson, and R. Kesavamoorthy, Diffraction in crystalline colloidal-array photonic crystals, Phys. Rev. E **69**, 066619 (2004).

[5] T. Ruhl, P. Spahn, and G. P. Hellmann, Artificial opals prepared by melt compression, Polymer **44**, 7625 (2003).

[6] O. L. J. Pursiainen, J. J. Baumberg, H. Winkler, B. Viel, and T. Ruhl, Compact strain-sensitive flexible photonic crystals for sensors, Appl. Phys. Lett. **87**, 101902 (2005).

[7] O. L. J. Pursiainen, J. J. Baumberg, H. Winkler, B. Viel, P. Spahn, and T. Ruhl, Nanoparticle-tuned structural colour from polymer opals, Opt. Express **15**, 9553 (2007).

[8] P. V. Braun, Colour without colourants, Nature **472**, 423 (2011).

[9] C. E. Finlayson and J. J. Baumberg, Polymer opals as novel photonic materials, Polym. Int. **62**, 1403 (2013).

[10] P. Spahn, C. E. Finlayson, W. Mbi Etah, D. R. E. Snoswell, J. J. Baumberg, and G. P. Hellmann, Modification of the refractive-index contrast in polymer opal films, J. Mater. Chem. **21**, 8893 (2011).

[11] H. S. Wong, M. Mackley, S. Butler, J. J. Baumberg, D. R. E. Snoswell, C. E. Finlayson, and Q. Zhao, The rheology and processing of "edge sheared" colloidal polymer opals, J. Rheol. **58**, 397 (2014).

[12] D. R. E. Snoswell, A. Kontogeorgos, J. J. Baumberg, T. D. Lord, M. R. Mackley, P. Spahn, and G. P. Hellmann, Shear ordering in polymer photonic crystals, Phys. Rev. E **81**, 020401 (2010).

[13] A. Kontogeorgos, D. R. E. Snoswell, C. E. Finlayson, J. J. Baumberg, P. Spahn, and G. P. Hellmann, Inducing Symmetry Breaking in Nanostructures: Anisotropic Stretch-Tuning Photonic Crystals, Phys. Rev. Lett. **105**, 233909 (2010).

[14] C. E. Finlayson, P. Spahn, D. R. E. Snoswell, G. Yates, A. Kontogeorgos, A. I. Haines, G. P. Hellmann, and J. J. Baumberg, 3D bulk ordering in macroscopic solid opaline films by edge-induced rotational shearing, Adv. Mater. **23**, 1540 (2011).

[15] O. L. J. Pursiainen, J. J. Baumberg, H. Winkler, B. Viel, P. Spahn, and T. Ruhl, Shear-induced organization in flexible polymer opals, Adv. Mater. **20**, 1484 (2008).

[16] D. R. E. Snoswell and J. J. Baumberg, Stretching the imagination, Textiles **4**, 8 (2009).

[17] J. Sussman, D. R. E. Snoswell, A. Kontogeorgos, J. J. Baumberg, and P Spahn, Thermochromic polymer opals, Appl. Phys. Lett. **95**, 173116 (2009).

[18] Y. Imai, C. E. Finlayson, P. Goldberg-Oppenheimer, Q. Zhao, P. Spahn, D. R. E. Snoswell, A. I. Haines, G. P. Hellmann, and

J. J. Baumberg, Electrically conductive polymer photonic crystals, Soft Matter **8**, 6280 (2012).
[19] C. E. Finlayson, D. R. E. Snoswell, P. Spahn, and J. J. Baumberg, Stretching polymer opal fibers tunes structural color, Laser Focus World **47**, 43 (2011).
[20] C. G. Schäfer, M. Gallei, J. T. Zahn, J. Engelhardt, G. P. Hellmann, and M. Rehahn, Reversible light-, thermo-, and mechano-responsive elastomeric polymer opal films, Chem. Mater. **25**, 2309 (2013).
[21] B. J. Ackerson, Shear induced order and shear processing of model hard sphere suspensions, J. Rheol. **34**, 553 (1990).
[22] B. J. Ackerson and P. N. Pusey, Shear-Induced Order in Suspensions of Hard Spheres, Phys. Rev. Lett. **61**, 1033 (1988).
[23] R. M. Amos, J. G. Rarity, P. R. Tapster, and T. J. Shepherd, Fabrication of large-area face-centered-cubic hard-sphere colloidal crystals by shear alignment, Phys. Rev. E **61**, 2929 (2000).
[24] J. Liu, D. A. Weitz, and B. J. Ackerson, Coherent crystallography of shear-aligned crystals of hard-sphere colloids, Phys. Rev. E **48**, 1106 (1993).
[25] M. D. Haw, W. C. K. Poon, and P. N. Pusey, Direct observation of oscillatory-shear- induced order in colloidal suspensions, Phys. Rev. E **57**, 6859 (1998).
[26] J. Vermant and M. J. Solomon, Flow-induced structure in colloidal suspensions, J. Phys.: Condens. Matter **17**, R187 (2005).
[27] Y. D. Yan, J. K. G. Dhont, C. Smits, and H. N. W. Lekkerkerker, Oscillatory-shear- induced order in non-aqueous dispersions of charged colloidal spheres, Physica A **202**, 68 (1994).
[28] J. Zhu, M. Li, R. Rogers, W. Meyer, R. H. Ottewill, STS-73 Space Shuttle Crew, W. B. Russel, and P. M. Chaikin, Crystallization of hard-sphere colloids in microgravity, Nature **387**, 883 (1997).
[29] B. Viel, T. Ruhl, and G. P. Hellmann, Reversible deformation of opal elastomer, Chem. Mater. **19**, 5673 (2007).
[30] http://www.linkam.co.uk/css450-specifications.
[31] A. I. Haines, C. E. Finlayson, D. R. E. Snoswell, P. Spahn, G. P. Hellmann, and J. J. Baumberg, Anisotropic resonant scattering from polymer photonic crystals, Adv. Mater. **24**, OP305 (2012).
[32] C. E. Finlayson, A. I. Haines, D. R. E. Snoswell, A. Kontogeorgos, S. Vignolini, J. J. Baumberg, P. Spahn, and G. P. Hellmann, Interplay of index contrast with periodicity in polymer photonic crystals, Appl. Phys. Lett. **99**, 261913 (2011).
[33] P. Ossi, *Disordered Materials* (Springer-Verlag, Heidelberg, Germany, 2006).
[34] See Supplemental Material at http://link.aps.org/supplemental/10.1103/PhysRevE.92.052315 for videos showing the shear cell with polymer opal samples under the complete shearing cycle.
[35] N. Koumakis, A. B. Schofield, and G. Petekidis, Effects of shear induced crystallization on the rheology and ageing of hard sphere glasses, Soft Matter **4**, 2008 (2008).
[36] Y. L. Wu, D. Derks, A. van Blaaderen, and A. Imhof, Melting and crystallization of colloidal hard-sphere suspensions under shear, Proc. Natl. Acad. Sci. USA **106**, 10564 (2009).
[37] B. Lander, U Seifert, and T. Speck, Crystallization in a sheared colloidal suspension, J. Chem. Phys. **138**, 224907 (2013).
[38] C. C. Miller, The Stokes-Einstein law for diffusion in solution, Proc. R. Soc. London, Ser. A, **106**, 724 (1924).
[39] P. Panine, T. Naranyan, J. Vermant, and J. Mewis, Structure and rheology during shear-induced crystallization of a latex suspension, Phys. Rev. E **66**, 022401 (2002).
[40] C. E. Finlayson, C. Goddard, E. Papachristodoulou, D. R. E Snoswell, A. Kontogeorgos, P. Spahn, G. P. Hellmann, O. Hess, and J. J Baumberg, Ordering in stretch tunable polymeric opal fibers, Opt. Express **19**, 3144 (2011).
[41] Q. Zhao, Ph.D. thesis, Oscillatory Shearing in Polymer Opals, University of Cambridge, 2015.
[42] A. A. Catherall, J. R. Melrose, and R. C. Ball, Shear thickening and order-disorder effects in concentrated colloids at high shear rates, J. Rheol. **44**, 1 (2000).